

---

# $k$ -Mixup Regularization for Deep Learning via Optimal Transport

---

**Kristjan Greenewald**  
MIT-IBM Watson AI Lab  
kristjan.h.greenewald@ibm.com

**Anming Gu**  
Boston University

**Mikhail Yurochkin**  
IBM Research

**Justin Solomon**  
MIT

**Edward Chien**  
Boston University

## Abstract

Mixup is a popular regularization technique for training deep neural networks that can improve generalization and increase adversarial robustness. It perturbs input training data in the direction of other randomly-chosen instances in the training set. To better leverage the structure of the data, we extend mixup to  $k$ -mixup by perturbing  $k$ -batches of training points in the direction of other  $k$ -batches using displacement interpolation, interpolation under the Wasserstein metric. We demonstrate theoretically and in simulations that  $k$ -mixup preserves cluster and manifold structures, and we extend theory studying efficacy of standard mixup. Our empirical results show that training with  $k$ -mixup further improves generalization and robustness on benchmark datasets.

## 1 Introduction

Deep neural networks have led to revolutionary performance advances in computer vision, speech recognition, reinforcement learning, and other applied machine learning domains [1, 2, 3, 4, 5]. A persistent issue, however, has been their tendency to memorize training data [6], due to their large parameter space. Memorization can lead to poor generalization and robustness to adversarial attack or label corruption [7]. Recently, mixup [8] and its variants [9, 10, 11, 12] have been applied to regularize training and address these problems. The resulting benefits have also been leveraged in the semi-supervised setting [13, 14] and applied to training of fair classifiers [15].

Standard mixup [8] is a data augmentation approach that trains models on weighted averages of random pairs of training points. Averaging weights are typically drawn from a beta distribution  $\beta(\alpha, \alpha)$ , with parameter  $\alpha \ll 1$  such that the generated training set is *vicinal*, i.e., it does not stray too far from the original dataset. Perturbations generated by mixup may be in the direction of *any* other datapoint instead of being informed by local distributional structure. As shown in Figure 1, this is a key weakness of mixup that can lead to poor regularization when distributions are clustered or supported on an embedded manifold. With larger  $\alpha$ , the procedure can result in averaged training points with incorrect labels in other clusters or in locations that stray far from the data manifold.

To address these issues, we present an extension called  $k$ -mixup, which averages random pairs of *sets* of  $k$  samples from the training dataset. This averaging is done using optimal transport, with *displacement interpolation*. The sets of  $k$  samples are viewed as discrete distributions and are averaged as distributions in a geometric sense. If  $k = 1$ , we recover standard mixup regularization. Figure 1 illustrates how  $k$ -mixup produces perturbed training datasets that better match the global cluster or manifold support structure of the original training dataset. In Section 5, we provide empirical results that justify the above intuition.

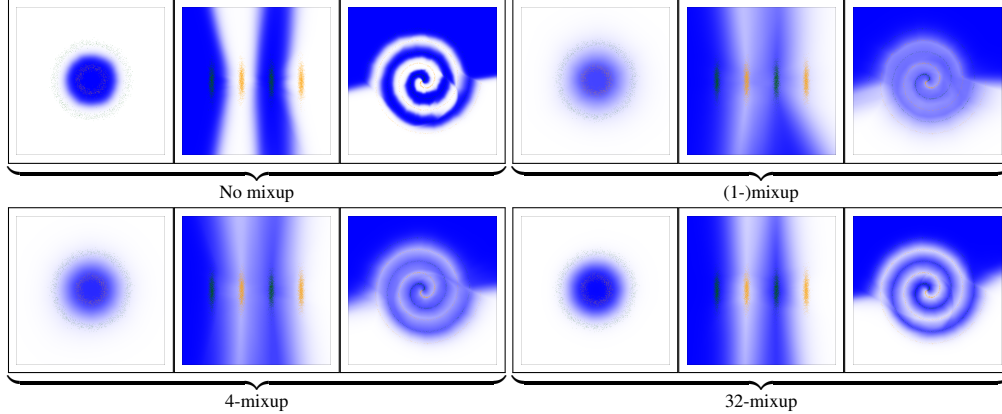


Figure 1: We train a fully-connected network on three synthetic datasets for binary classification, with 1-mixup through 32-mixup regularization ( $\alpha = 1$ ). The plotted functions show the network output and demonstrate that higher  $k$ -mixup better captures local structure (visible through less blur, increased contrast) while retaining reasonable, even smoothing between the classes.

Our contributions are as follows.

- Empirical results:
  - We show improved generalization results on standard benchmark datasets showing  $k$ -mixup with  $k > 1$  often improves on standard mixup and at worst does no harm.
  - We show that  $k$ -mixup further improves robustness to adversarial attacks.
- Theoretical characterizations that speak to the claims above in a more precise manner:
  - We argue that as  $k$  increases, one is more and more likely to remain within the data manifold (Section 3.1).
  - In the clustered setting, we provide an argument that shows intercluster regularization interpolates nearest points and better smooths interpolation of labels (Section 3.2).
  - We extend the theoretical analysis of [16, 17] to our  $k$ -mixup setting, showing that it leverages local training distribution structure to make more informed regularizations (Section 4).

**Related works.** We tackle issues noted in the papers on adaptive mixup [10] and manifold mixup [9]. The first refers to the problem as “manifold intrusion” and seeks to fix it by training datapoint-specific weights  $\alpha$  and considering convex combinations of more than 2 points. This requires additional networks to detect the data manifold and to assign weight combinations, adding substantial complexity to their approach. Manifold mixup deals with the problem by relying on the network to parametrize the data manifold, interpolating in hidden layers of the network. We show in Section 5 that  $k$ -mixup can be performed in hidden layers to boost performance of manifold mixup.

PuzzleMix [12] also combines optimal transport ideas with mixup, extending CutMix [11] to combine pairs of images. PuzzleMix uses transport to shift saliency regions of images, producing meaningful combinations of input training data. Their use of OT is fundamentally different from ours and does not generalize to non-image data. A recent follow-on work CoMix [18], considers a similar approach based on sub/supermodular optimization.

## 2 Generalizing Mixup

**Standard mixup.** Mixup considers a training dataset of feature-target pairs  $\{(x_i, y_i)\}_{i=1}^N$ ; the target  $y_i$  is a one-hot vector for classification. Weighted averages of training points construct a vicinal dataset:

$$(\tilde{x}_{ij}^\lambda, \tilde{y}_{ij}^\lambda) := (\lambda x_i + (1 - \lambda)x_j, \lambda y_i + (1 - \lambda)y_j).$$

The weight  $\lambda$  is sampled from a beta distribution,  $\beta(\alpha, \alpha)$ , with parameter  $\alpha > 0$  typically taken to be small and less than 1, so that the weighted averages are near an endpoint. With the model trained on such a vicinal dataset, the mixup-regularized empirical risk minimization (ERM) objective is:

$$\mathcal{E}_1^{mix}(f) := \mathbb{E}_{i,j,\lambda} [\ell(f(\tilde{x}_{ij}^\lambda), \tilde{y}_{ij}^\lambda)], \quad i, j \sim \mathcal{U}\{1, \dots, N\}, \lambda \sim \beta(\alpha, \alpha), \quad (1)$$

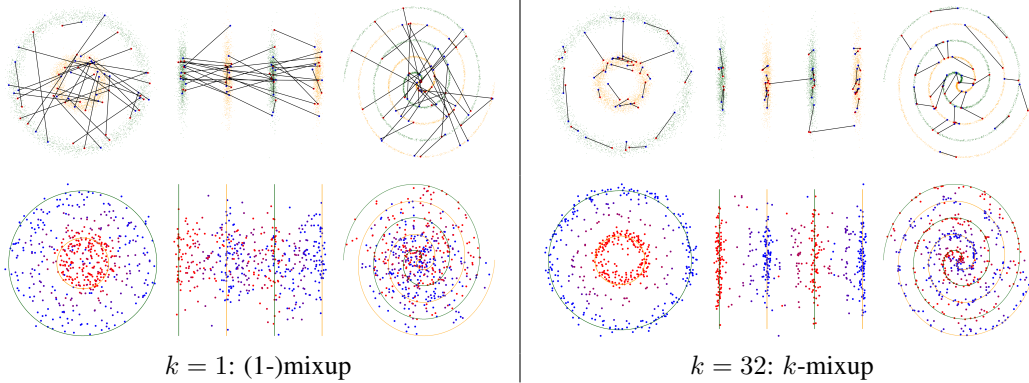


Figure 2: Optimal transport couplings and vicinal datasets for  $k = 1$  (left) and  $k = 32$  (right) in 3 simple datasets. In the bottom row,  $\alpha = 1$  was used to generate vicinal datasets of size 512.

where  $f$  is a proposed feature-target map and  $\ell$  is a loss function. Effectively, one trains on datasets formed by averaging random pairs of training points. As the training points are randomly selected, this construction makes it likely that the vicinal datapoints may not reflect the local structure of the dataset, as in the clustered or manifold-support setting.

**$k$ -mixup.** To generalize mixup, we sample two random subsets of  $k$  training points  $\{(x_i^\gamma, y_i^\gamma)\}_{i=1}^k$  and  $\{(x_i^\xi, y_i^\xi)\}_{i=1}^k$ . For compactness, let  $x^\gamma := \{x_i^\gamma\}_{i=1}^k$  and  $y^\gamma := \{y_i^\gamma\}_{i=1}^k$  denote the feature and target sets (and likewise for  $\xi$ ). A weighted average of these subsets is formed with *displacement interpolation* and used as a vicinal training set. This concept is from optimal transport (see, e.g., [19]) and considers  $(x^\gamma, y^\gamma)$  and  $(x^\xi, y^\xi)$  as uniform discrete distributions  $\hat{\mu}^\gamma, \hat{\mu}^\xi$  over their support. In this setting, the optimal transport problem becomes a linear assignment problem [20]. The optimal map is described by a permutation  $\sigma \in S_k$  minimizing the cost:

$$W_2^2(\hat{\mu}^\gamma, \hat{\mu}^\xi) = \frac{1}{k} \sum_{i=1}^k \|x_i^\gamma - x_{\sigma(i)}^\xi\|_2^2.$$

Here,  $\sigma$  can be found efficiently using the Hungarian algorithm [21]. Figure 2 gives intuition for this identification. When compared to the random matching used by standard mixup, our pairing is more likely to match nearby points and to make matchings that better respect local structure—especially by having cross-cluster matches between nearby points on the two clusters.

Given a permutation  $\sigma$  and an averaging weight  $\lambda$ , we define the displacement interpolation between  $(x^\gamma, y^\gamma)$  and  $(x^\xi, y^\xi)$  by:

$$DI_\lambda((x^\gamma, y^\gamma), (x^\xi, y^\xi)) := \left\{ \lambda(x_i^\gamma, y_i^\gamma) + (1 - \lambda)(x_{\sigma(i)}^\xi, y_{\sigma(i)}^\xi) \right\}_{i=1}^k.$$

As in standard mixup, we draw  $\lambda \sim \beta(\alpha, \alpha)$ . For the loss function, we consider all  $\binom{N}{k}$  subsets of  $k$  random samples, i.e.,  $\{\{(x_i^\gamma, y_i^\gamma)\}_{i=1}^k\}_{\gamma=1}^{\binom{N}{k}}$ :

$$\mathcal{E}_k^{mix}(f) = \mathbb{E}_{\gamma, \xi, \lambda} [\ell(f(DI_\lambda(x^\gamma, x^\xi)), DI_\lambda(y^\gamma, y^\xi))], \quad \gamma, \xi \sim \mathcal{U}\{1, \dots, \binom{N}{k}\}, \lambda \sim \beta(\alpha, \alpha).$$

Due to the localized nature of the matchings, particularly the fact that cross-cluster matches tend to be approximately bisected by the decision boundary, the average (displacement) interpolated vicinal distribution will likely be closer to the ideal case where the averaged labels correspond to the point's relative position in the voids between the classes. A consequence is that  $k$ -mixup is robust to higher values of  $\alpha$ , since it is no longer necessary to keep  $\lambda$  close to 0 or 1 to avoid erroneous labels. This can be seen in our empirical results in Section 5, and theoretical analysis appears in Section 4.

**Computational cost.** While the cost of the Hungarian algorithm grows as  $O(k^3)$ , it yields  $k$  data points for regularization, yielding an amortized  $O(k^2)$  complexity per data point. For the values of  $k$  we consider, however, this cost remains small relative to that of gradient computation (e.g. for parameters of Resnet-18 and others). Moreover, training convergence speed is unaffected, unlike manifold mixup [9], which in our experience converges slower and has larger computational overhead. Overall, there is little computational downside to generalizing 1-mixup to  $k$ -mixup.

### 3 Manifold and Cluster Structure Preservation

The use of an optimal coupling for producing vicinal data points makes it likely that vicinal datapoints reflect the local structure of the dataset. Below we argue that as  $k$  increases, the vicinal couplings will preserve manifold support, preserve cluster structure, and interpolate labels between clusters.

#### 3.1 Manifold support

Suppose our training data is drawn from a distribution  $\mu$  on a  $d$ -dimensional embedded submanifold  $\mathcal{S}$  in  $\mathcal{X} \times \mathcal{Y} \subset \mathbb{R}^M$ , where  $\mathcal{X}$  and  $\mathcal{Y}$  denote feature and target spaces. We define an injectivity radius:

**Definition 1** (Injectivity radius). *Let  $B_\epsilon(\mathcal{S}) = \{p \in \mathcal{X} \times \mathcal{Y} \mid d(p, \mathcal{S}) < \epsilon\}$  denote the  $\epsilon$ -neighborhood of  $\mathcal{S}$  where  $d(p, \mathcal{S})$  is the Euclidean distance from  $p$  to  $\mathcal{S}$ . Define the injectivity radius  $R_\mathcal{S}$  of  $\mathcal{S}$  to be the infimum of the  $\epsilon$ 's for which  $B_\epsilon(\mathcal{S})$  is not homotopy equivalent to  $\mathcal{S}$ .*

As  $\mathcal{S}$  is embedded,  $B_\epsilon(\mathcal{S})$  is homotopy equivalent to  $\mathcal{S}$  for small enough  $\epsilon$ , so  $R_\mathcal{S} > 0$ . Essentially, Definition 1 grows an  $\epsilon$  neighborhood until the boundary intersects itself. We have the following:

**Proposition 1.** *For a training distribution  $\mu$  supported on an embedded submanifold  $\mathcal{S}$  with injectivity radius  $R_\mathcal{S}$ , with high probability any constant fraction  $1 - \delta$  (for any fixed  $\delta \in (0, 1]$ ) of the couplings induced by  $k$ -mixup will remain within  $B_\epsilon(\mathcal{S})$ , for  $k$  large enough.*

*Proof.* Finite-sample convergence of empirical measures implies that for an arbitrary sampling of  $k$  points  $\hat{\mu}_k$ , we have  $W_2^2(\mu, \hat{\mu}_k) \leq O(k^{-2/d})$  with high probability (e.g.,  $1 - 1/k^2$  probability, from Theorem 9.1 of [22] when combined with results from [23]). The triangle inequality then implies that the Wasserstein-2 distance between our batches of  $k$  samples will tend to 0 at the same asymptotic rate:  $W_2^2(\hat{\mu}_k^\gamma, \hat{\mu}_k^\xi) \leq O(k^{-2/d})$  with high probability.

Recalling that by the definition of the optimal coupling permutation  $\sigma(i)$ , we have  $\frac{1}{k} \sum_{i=1}^k \|x_i^\gamma - x_{\sigma(i)}^\xi\|_2^2 = W_2^2(\hat{\mu}_k^\gamma, \hat{\mu}_k^\xi) \leq O(k^{-2/d})$  with high probability. Hence, for any  $\mathcal{I} \subseteq [1, k]$  with  $\|x_i^\gamma - x_{\sigma(i)}^\xi\|_2^2 > k^{-1/d}$  for all  $i \in \mathcal{I}$ ,  $|\mathcal{I}| \leq O(k^{1-1/d}) \leq \delta k$  for  $k$  large enough and any  $\delta \in (0, 1]$ . In essence, long-distance identifications are rare, and their fraction is bounded for large enough  $k$ . Therefore, for  $k$  large enough, again with high probability there exists a subset  $\tilde{\mathcal{I}}$  with  $|\tilde{\mathcal{I}}| \geq (1 - \delta)k$  such that  $\|x_i^\gamma - x_{\sigma(i)}^\xi\|_2 \leq R_\mathcal{S}$  for all  $i \in \tilde{\mathcal{I}}$ . Since  $x_i^\gamma$  and  $x_{\sigma(i)}^\xi$  lie in  $\mathcal{S}$ , the proposition results.  $\square$

Hence, for large enough  $k$ , the interpolation induced by optimal transport will approximately preserve the manifold support structure. While the theory requires low dimension  $d$  and high  $k$  to achieve a tight bound, our empirical evaluations show good performance in the small- $k$  regime.

#### 3.2 Clustered distributions

With a clustered training distribution, we preserve global structure in two ways: by mostly matching points within clusters and by matching (approximately) nearest points across clusters. These characterizations will only be true approximately, but will be achieved exactly as  $k \rightarrow \infty$ , as argued below.

To refine the definition of a clustered distribution, we adopt the  $(m, \Delta)$ -clusterable definition used in [23, 22]. In particular, a distribution  $\mu$  is  $(m, \Delta)$ -clusterable if  $\text{supp}(\mu)$  lies in the union of  $m$  balls of radius at most  $\Delta$ . Now, if our training samples  $(x_i, y_i)$  are sampled from such a distribution, where the clusters are sufficiently separated, then intracluster matchings will be prioritized over cross-cluster matchings under optimal transport.

**Lemma 1.** *Draw two batches of samples  $\{p_i\}_{i=1}^N$  and  $\{q_i\}_{i=1}^N$  from a  $(m, \Delta)$ -clusterable distribution, where the distance any pair of covering balls is at least  $2\Delta$ . If  $r_i$  and  $s_i$  denote the number of samples in cluster  $i$  in batch 1 and 2, respectively, then the optimal transport matching will have  $\frac{1}{2} \sum_i |r_i - s_i|$  cross-cluster matchings.*

The proof of the above (supplement Section A) involves the pigeonhole principle and basic geometry.

We now argue that the fraction of cross-cluster identifications approaches zero as  $k \rightarrow \infty$  and characterize the rate of decrease. The proof (supplement Section B) follows from Jensen's inequality:

**Theorem 1.** Given a distribution with  $m$  clusters, with probability masses  $p_1, \dots, p_m$ , and two batches of size  $k$  matched with optimal transport, the expected fraction of cross-cluster identifications is  $O\left(\frac{\sum_{i=1}^m \sqrt{p_i(1-p_i)}}{\sqrt{2k}}\right)$ .

Finally, we show that matches between well-separated clusters are of length close to the distance between the clusters with high probability (proved in supplement Section C), i.e., the endpoints of the match lie in the parts of each cluster closest to the other cluster. This rests upon the fact that we are considering the  $W_2$  cost, for which small improvements to long distance matchings yield large cost reductions in squared Euclidean distance.

**Theorem 2.** Suppose density  $p$  has support on disjoint compact sets (clusters)  $A, B$  whose boundaries are smooth, where  $p > 0$  throughout  $A$  and  $B$ . Let  $D$  be the Euclidean distance between  $A$  and  $B$ , and let  $R_A, R_B$  be the radii of  $A, B$  respectively. Define  $A_\epsilon$  to be the subset of set  $A$  that is less than  $D(1 + \epsilon)$  distance from  $B$ , and define  $B_\epsilon$  similarly. Consider two batches of size  $k$  drawn from  $p$  and matched with optimal transport. Then, for  $k$  large enough, with high probability all cross-cluster matches will have an endpoint each in  $A_\epsilon$  and  $B_\epsilon$ , where  $\epsilon = \frac{\max(R_A, R_B)^2}{D^2}$ .

Theorem 2 implies for large  $k$  that the vicinal distribution created by sampling along the cross-cluster matches will almost entirely lie in the voids between the clusters. If the clusters correspond to different classes, this will directly encourage the learned model to smoothly interpolate between the class labels as one transitions across the void between clusters. This is in contrast to the randomized matches of 1-mixup, which create vicinal distributions that can span a line crossing any part of the space without regard for intervening clusters. Lastly, a naïve interpolation between a datapoint and its nearest neighbor in a batch would not produce any cross-cluster matchings and would not provide any information in the voids between clusters.

## 4 Regularization Expansions

Two recent works analyze the efficacy of 1-mixup perturbatively [16, 17]. Both consider quadratic Taylor series expansions about the training set or a simple transformation of it, and they characterize the regularization terms that arise in terms of label and Lipschitz smoothing. We adapt these expansions to  $k$ -mixup and show that the resulting regularization is more locally informed via the optimal transport coupling.

In both works, perturbations are sampled from a globally informed distribution, based upon all other samples in the training distribution. In  $k$ -mixup, these distributions are defined by the optimal transport couplings. Given a training point  $x_i$ , let us consider all  $k$ -samplings  $\gamma$  that might contain it, and all possible  $k$ -samplings  $\xi$  that we might couple it to. A locally-informed distribution is the following:

$$\mathcal{D}_i := \frac{1}{\binom{N-1}{k-1} \binom{N}{k}} \sum_{\gamma=1}^{\binom{N-1}{k-1}} \sum_{\xi=1}^{\binom{N}{k}} \delta \sigma_{\gamma\xi}(x)$$

where  $\sigma_{\gamma\xi}$  denotes the optimal coupling between  $k$ -samplings  $\gamma$  and  $\xi$ . This distribution will be more heavily weighted on points that  $x$  is often matched with.

In [16], the authors expand about the features in the training dataset  $\mathcal{D}_X := \{x_1, \dots, x_n\}$ , and the perturbations in the regularization terms are sampled from  $\mathcal{D}$ . We can generalize their characterization to  $k$ -mixup, with  $\mathcal{D}$  replaced by  $\mathcal{D}_i$ . In particular, let us assume that our loss is of the form  $\ell(f(x), y) = h(f(x)) - y \cdot f(x)$  for some twice differentiable  $h$  and  $f$ . This broad class of losses includes the cross-entropy for neural networks and all losses arising from Generalized Linear Models.

**Theorem 3.** Assuming a loss  $\ell$  as above, the  $k$ -mixup loss can be written as:

$$\mathcal{E}_k^{mix}(f) = \mathcal{E}^{std} + \sum_{i=1}^3 \mathcal{R}_i + \mathbb{E}_{\lambda \sim \beta(\alpha+1, \alpha)} [(1-\lambda)^2 \phi(1-\lambda)]$$

where  $\lim_{a \rightarrow 0} \phi(a) = 0$ ,  $\mathcal{E}^{std}$  denotes the standard ERM loss, and the three  $\mathcal{R}_i$  regularization terms are:

$$\begin{aligned}\mathcal{R}_1 &= \frac{\mathbb{E}_{\lambda \sim \beta(\alpha+1, \alpha)} [1 - \lambda]}{n} \sum_{i=1}^N (h'(f(x_i)) - y_i) \nabla f(x_i)^T \mathbb{E}_{r \sim \mathcal{D}_i} [r - x_i] \\ \mathcal{R}_2 &= \frac{\mathbb{E}_{\lambda \sim \beta(\alpha+1, \alpha)} [(1 - \lambda)^2]}{2n} \sum_{i=1}^N h''(f(x_i)) \nabla f(x_i)^T \mathbb{E}_{r \sim \mathcal{D}_i} [(r - x_i)(r - x_i)^T] \nabla f(x_i) \\ \mathcal{R}_3 &= \frac{\mathbb{E}_{\lambda \sim \beta(\alpha+1, \alpha)} [(1 - \lambda)^2]}{2n} \sum_{i=1}^N (h'(f(x_i)) - y_i) \mathbb{E}_{r \sim \mathcal{D}_i} [(r - x_i) \nabla^2 f(x_i) (r - x_i)^T].\end{aligned}$$

A proof is given in Section D of the supplement and follows from some algebraic rearrangement and a Taylor expansion in terms of  $1 - \lambda$ .  $\mathcal{E}^{std}$  represents the constant term in this expansion, while the regularization terms  $\mathcal{R}_i$  represent the linear and quadratic terms. These effectively regularize  $\nabla f(x_i)$  and  $\nabla^2 f(x_i)$  with respect to local perturbations  $r - x_i$  sampled from  $\mathcal{D}_i$ . The higher-order terms are captured by  $\mathbb{E}_{\lambda \sim \beta(\alpha+1, \alpha)} [(1 - \lambda)^2 \phi(1 - \lambda)]$ . Notably, the expansion is in the feature space alone, yielding theoretical results in the case of 1-mixup on generalization and adversarial robustness.

[17] characterizes mixup as a combination of a reversion to mean followed by random perturbation. We generalize their result with a locally-informed mean as follows:

**Theorem 4.** Define  $(\tilde{x}_i^\gamma, \tilde{y}_i^\gamma)$  as

$$\begin{aligned}\tilde{x}_i^\gamma &= \bar{x}_i^\gamma + \bar{\theta}(x_i^\gamma - \bar{x}_i^\gamma) \\ \tilde{y}_i^\gamma &= \bar{y}_i^\gamma + \bar{\theta}(y_i^\gamma - \bar{y}_i^\gamma),\end{aligned}$$

where  $\bar{x}_i^\gamma = \frac{1}{\binom{N}{k}} \sum_{\xi=1}^{\binom{N}{k}} x_{\sigma_{\gamma\xi}(i)}^\xi$  and  $\bar{y}_i^\gamma = \frac{1}{\binom{N}{k}} \sum_{\xi=1}^{\binom{N}{k}} y_{\sigma_{\gamma\xi}(i)}^\xi$  are expectations under the matchings and  $\theta \sim \beta_{[1/2, 1]}(\alpha, \alpha)$ . Further, denote the zero mean perturbations

$$\begin{aligned}\tilde{\delta}_i^\gamma &= (\theta - \bar{\theta})x_i^\gamma + (1 - \theta)x_{\sigma_{\gamma\xi}(i)}^\xi - (1 - \bar{\theta})\bar{x}_i^\gamma \\ \tilde{\epsilon}_i^\gamma &= (\theta - \bar{\theta})y_i^\gamma + (1 - \theta)y_{\sigma_{\gamma\xi}(i)}^\xi - (1 - \bar{\theta})\bar{y}_i^\gamma.\end{aligned}$$

Then the  $k$ -mixup loss can be written as

$$\mathcal{E}_k^{OTmixup}(f) = \frac{1}{\binom{N}{k}} \sum_{\gamma=1}^{\binom{N}{k}} \mathbb{E}_{\theta, \xi} \left[ \frac{1}{k} \sum_{i=1}^k \ell(\tilde{y}_i^\gamma + \tilde{\epsilon}_i^\gamma, f(\tilde{x}_i^\gamma + \tilde{\delta}_i^\gamma)) \right].$$

A proof is given in supplementary Section E. The mean  $\bar{x}_i^\gamma$  being shifted toward is exactly the mean of the locally-informed distribution  $\mathcal{D}_i$ . Moreover, the covariance structure of the perturbations is detailed in the supplementary and is now also derived from the local structure of the distribution, inferred from the optimal transport matchings.

## 5 Results

We empirically test the efficacy of  $k$ -mixup with toy datasets, UCI datasets, and image datasets. Across these experiments we find that  $k$ -mixup for  $k > 1$  tends to improve upon (1-)mixup for fixed  $\alpha$ , and if not remains comparable. Additional experiments with CIFAR-10 compare  $k$ -mixup with manifold mixup, explore the combination of the two methods, and demonstrate improvements in adversarial robustness from  $k$ -mixup. Experiments were performed in various laptop, cluster, and cloud environments using PyTorch. Unless otherwise stated, a standard SGD optimizer was used, with learning rate 0.1 decreased at epochs 100 and 150, momentum 0.9, and weight decay  $10^{-4}$ .

**Toy datasets.** Results for the toy datasets of Figures 1 and 2 (denoted ‘‘One Ring,’’ ‘‘Four Bars,’’ and ‘‘Swiss Roll’’) are shown in Figure 3. We used a fully-connected 3-layer neural network (130 and 120 hidden units). For each dataset and each  $\alpha$ , higher  $k$ -mixup outperforms (1-)mixup. For larger  $\alpha$ , the performance gap between the baseline (1-)mixup and  $k > 1$  mixup becomes quite significant,

$k$	$\alpha = .25$	$\alpha = 1$	$\alpha = 4$	$\alpha = 16$	$\alpha = 64$	$\alpha = .25$	$\alpha = 1$	$\alpha = 4$	$\alpha = 16$	$\alpha = 64$	$\alpha = .25$	$\alpha = 1$	$\alpha = 4$	$\alpha = 16$	$\alpha = 64$
1	94.487	90.930	86.527	86.467	86.899	100	100	100	50.110	50.017	99.708	99.670	67.942	61.633	59.573
2	95.230	93.197	90.653	90.043	90.027	100	100	100	60.725	50.107	99.653	99.667	81.696	69.327	64.397
4	96.190	94.110	92.633	92.191	91.807	100	100	100	98.750	92.477	99.703	<b>99.717</b>	<b>99.721</b>	80.064	73.773
8	96.547	95.714	94.377	93.807	93.463	100	100	100	99.920	99.853	99.693	99.69	99.646	99.710	98.897
16	<b>96.717</b>	<b>95.961</b>	<b>95.097</b>	<b>95.017</b>	<b>95.193</b>	100	100	100	<b>99.997</b>	<b>99.987</b>	<b>99.760</b>	99.707	99.692	<b>99.787</b>	<b>99.761</b>

(a) One Ring

(b) Four Bars

(c) Swiss Roll

Figure 3: % correct classification on test data for toy datasets, averaged over 5 Monte Carlo trials.

	None	$k = 1$	$k = 5$	$k = 10$		None	$k = 1$	$k = 2$	$k = 4$	$k = 8$	$k = 16$	$k = 32$	$k = 64$
$\alpha = 1$	92.0	98.0	94.0	<b>100.0</b>	$\alpha = 1$	91.4	89.8	93.7	90.6	<b>95.3</b>	93.7	92.1	94.5

(a) Iris (% correct classification on test data)

(b) Breast Cancer Wisconsin-Diagnostic (% correct classification on test data)

	$\alpha = 1$	None	$k = 1$	$k = 2$	$k = 4$	$k = 8$
Abalone	27.58	27.93	27.67	27.77	<b>28.43</b>	
Arrhythmia	64.57	61.96	<b>66.30</b>	64.02	65.00	
HTRU2	97.60	97.60	97.65	97.55	<b>97.71</b>	
Phishing	96.12	95.72	96.19	96.06	<b>96.21</b>	

(c) Other datasets (% correct classification on test data)

Figure 4: Results for UCI datasets using fully connected networks.

reaching 8%, 50%, and 40% respectively for  $k = 16$  and  $\alpha = 64$ . These results quantitatively confirm the intuition built in Figures 1 and 2 that  $k$ -mixup regularization more effectively preserves these structures in data.

**UCI datasets.** Scaling up from toy datasets, we tried  $k$ -mixup on UCI datasets of varying size and dimension: Iris (150 instances, dim. 4), Breast Cancer Wisconsin-Diagnostic (569 instances, dim. 30), Abalone (4177 instances, dim. 8), Arrhythmia (452 instances, dim. 279), HTRU2 (17898 instances, dim. 9), and Phishing (11055 instances, dim. 30) UCI datasets. For Iris, we used a 3-layer network with 120 and 84 hidden units; for Breast Cancer, Abalone, and Phishing, we used a 4-layer network with 120, 120, and 84 hidden units; for Arrhythmia we used a 5-layer network with 120, 120, 36, and 84 hidden units; and lastly, for HTRU2, we used a 5 layer network with 120, 120, 84, 132 hidden units. We used  $\alpha = 1$  and each entry is averaged over 10 Monte Carlo trials. Test classification performance is shown in Figure 4.  $k$ -mixup improves over (1-)mixup or no mixup in each case (though the improvements in HTRU2 and Phishing are not statistically significant).

$k$	$\alpha = .05$	$\alpha = .1$	$\alpha = .2$	$\alpha = .5$	$\alpha = 1$	$\alpha = 10$	$\alpha = 100$	$k$	$\alpha = .05$	$\alpha = .1$	$\alpha = .2$	$\alpha = .5$	$\alpha = 1$	$\alpha = 10$	$\alpha = 100$
1	99.09	99.09	99.05	99.03	98.98	98.79	98.64	1	0.068	0.148	0.239	0.436	0.617	1.347	1.732
2	99.11	99.12	99.07	99.02	98.99	98.88	98.75	2	0.070	0.129	0.214	0.388	0.586	1.228	1.585
4	99.13	99.11	99.09	99.06	99.04	98.91	98.85	4	0.049	0.111	0.191	0.338	0.542	1.078	1.399
8	99.12	99.12	99.09	99.06	99.01	99.00	98.99	8	0.037	0.092	0.149	0.305	0.449	0.930	1.191
16	99.18	99.15	99.14	99.08	99.04	99.08	99.12	16	0.035	0.070	0.122	0.241	0.341	0.719	0.938
32	99.18	99.15	99.17	99.10	99.11	99.16	<b>99.18</b>	32	0.029	0.039	0.076	0.152	0.221	0.456	0.586

(a) Performance (% correct classification on test data)

(b) Average squared distance of vicinal distribution from training set

Figure 5: Results for MNIST with a LeNet architecture. Numbers averaged over 20 Monte Carlo trials ( $\pm 0.02$  confidence on test performance).

**Image datasets.** Results for MNIST [24] using a convolutional neural network, i.e., LeNet modified slightly to accommodate grayscale images, are in Figure 5, with a joint sweep over  $k$  and  $\alpha$ . Each table entry is averaged over 20 Monte Carlo trials. For each generated point in the vicinal distribution, we compute its closest squared distance to the matched pair from which it was generated. The results are averaged over the vicinal dataset and reported in part (b) of the figure. It shows that  $k$ -mixup yields significantly closer matches as  $k$  increases, causing the generated vicinal distribution to deviate less (in terms of squared distance) from the original training set. In spite of this lower variation, for each  $\alpha$  the best generalization performance is for some  $k > 1$ , with  $\alpha = 100$  yielding 99.18% accuracy for  $k = 32$  compared to 98.64% accuracy for  $k = 1$ . Generally, for fixed  $\alpha$ , increasing  $k$  improves performance for this dataset.

Figure 6 shows analogous results for CIFAR-10, using the PreAct Resnet-18 architecture as in [8]. Again  $k$ -mixup succeeds in finding matches that lie

$k$	$\alpha = .1$	$\alpha = .2$	$\alpha = .5$	$\alpha = 1$	$\alpha = 10$
1	76.54	77.22	77.88	77.76	74.88
2	76.54	77.38	78.19	<b>78.41</b>	76.09
4	76.55	77.36	77.94	78.25	76.51
8	76.51	77.18	77.82	78.03	76.69
16	76.43	77.08	77.77	77.87	76.86
32	76.29	76.93	77.51	77.54	76.90

CIFAR-100 performance ( $\pm 0.05$  confidence)

$k$	$\alpha = .1$	$\alpha = .2$	$\alpha = .5$	$\alpha = 1$	$\alpha = 10$
1	97.13	97.12	97.14	97.17	96.76
2	97.16	97.14	97.19	<b>97.29</b>	96.81
4	97.11	97.13	97.16	97.24	96.87
8	97.16	97.11	97.14	97.23	96.94
16	97.09	97.11	97.08	97.16	96.93
32	97.16	97.10	97.05	97.08	96.94

(b) SVHN performance ( $\pm 0.02$  confidence)Figure 8: % correct classification on test data for CIFAR-100 and SVHN, averaged over 20 Monte Carlo trials ( $\pm 0.03$  confidence on test performance).

$k$	$\alpha = .05$	$\alpha = .1$	$\alpha = .2$	$\alpha = .5$	$\alpha = 1$	$\alpha = 10$	$\alpha = 100$
1	94.785	95.025	95.27	95.645	95.63	94.82	94.085
2	94.8	94.92	95.285	95.645	95.79	95.105	94.14
4	94.76	94.99	95.3	95.65	95.745	95.205	94.315
8	94.79	94.925	95.255	95.625	<b>95.815</b>	95.285	94.61
16	94.68	94.98	95.215	95.595	95.735	95.33	94.92
32	94.74	94.905	95.11	95.465	95.675	95.375	95.165

(a) Performance (% correct classification on test data)

$k$	$\alpha = .05$	$\alpha = .1$	$\alpha = .2$	$\alpha = .5$	$\alpha = 1$	$\alpha = 10$	$\alpha = 100$
1	29.5	58.2	107.1	198.1	280.3	624.1	803.1
2	27.0	54.0	94.4	192.6	276.8	564.9	721.2
4	22.3	58.6	87.3	163.0	240.6	494.3	637.6
8	24.1	43.1	78.4	141.7	199.5	431.3	554.8
16	16.8	32.6	70.7	114.3	186.6	365.2	468.7
32	14.9	28.4	50.4	96.9	142.4	288.6	371.7

(b) Average squared distance of vicinal distribution from training set.

Figure 6: Results for CIFAR-10. Numbers averaged over 20 Monte Carlo trials ( $\pm .03$  confidence on test performance). Difference between best  $k$ -mixup and best 1-mixup is 0.17% for fixed high  $\alpha$  ( $\alpha = 100$ ), the improvement increases to 1.2%.

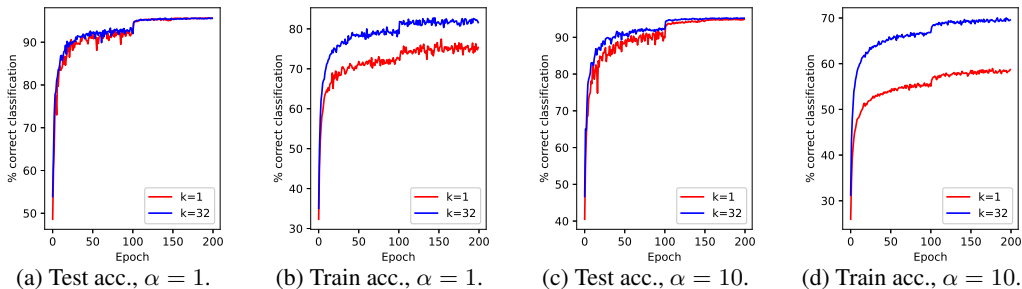


Figure 7: Training convergence of  $k = 1$  and  $k = 32$  mixup on CIFAR-10, averaged over 20 random trials. Note that both train at roughly the same rate ( $k = 32$  slightly faster), the train accuracy discrepancy is due to the more class-accurate vicinal training distribution created by higher  $k$ -mixup.

significantly closer together as  $k$  increases. For each  $\alpha$  except the small  $\alpha = .1$ , the best generalization performance is still for some  $k > 1$ , with  $\alpha = 100$  yielding 95.165% accuracy for  $k = 32$  compared to 94.085% accuracy for  $k = 1$ . While the best  $k$ -mixup performance exceeds that of the best 1-mixup by only 0.17%, recall that in this setting 1-mixup outperforms ERM by 1.4% [8], so when combined with the low overall error rate, small gains are not surprising.

Additionally, we show training curves (performance as a function of epoch) for CIFAR-10 in Figure 7, averaged over 20 random trials. The training speed (test accuracy in terms of epoch) for 1-mixup and 32-mixup shows no loss of convergence speed with  $k = 32$  mixup, with (if anything)  $k = 32$  showing a slight edge. The discontinuity at epoch 100 is due to our reduction of the learning rate at epochs 100 and 150 to aid convergence (used throughout our image experiments). The train accuracy shows similar convergence profile between 1- and 32-mixup; the difference in absolute accuracy here (and the reason it is less than the test accuracy) is because the training distribution is the mixup-modified vicinal distribution. The curve for  $k = 32$  is higher, especially for  $\alpha = 10$ , because the induced vicinal distribution and labels are more consistent with the true distribution, due to the better matches from optimal transport. The large improvement in train accuracy is remarkable given the high dimension of the CIFAR-10 data space, since it indicates that  $k = 32$  mixup is able to find significantly more consistent matches than  $k = 1$  mixup.

Figure 8 shows results for CIFAR-100 and SVHN, with a Resnet-18 architecture. As before, for fixed  $\alpha$ , the best performance is achieved for some  $k > 1$ . The improvement of the best  $k$ -mixup over the best 1-mixup is 0.53% for CIFAR-100 and 0.12% for SVHN. For fixed high  $\alpha = 10$ , the  $k$ -mixup improvement over 1-mixup rises to 2.02% for CIFAR-100, possibly indicating that the OT matches yield better interpolation between classes, aiding generalization.

**Manifold mixup.** We compare to Manifold Mixup [9], which helps in settings like those in Figure 1 by making interpolations more meaningful. It performs mixup at random layers (random per minibatch), not only in the input space. This extends to “manifold  $k$ -mixup:”  $k$ -mixup in the hidden layers as well as the input layers. We use settings in [9], i.e., for PreAct ResNet18, the mixup layer is randomized (coin flip) between the input space and the output of the first residual block.<sup>1</sup>

$k$	$\alpha = .1$	$\alpha = .2$	$\alpha = .5$	$\alpha = 1$	$\alpha = 10$
1	95.00	95.27	95.59	95.74	95.19
2	94.91	95.22	95.56	95.69	95.29
4	94.99	95.22	95.55	<b>95.75</b>	94.98
8	94.92	95.22	95.58	95.72	95.39
16	94.86	95.18	95.58	95.69	95.47
32	94.86	95.09	95.42	95.53	95.46

Figure 9: Manifold mixup.

<sup>1</sup>See [https://github.com/vikasverma1077/manifold\\_mixup](https://github.com/vikasverma1077/manifold_mixup)



$k$	$\epsilon=.5$	$\epsilon=1$	$\epsilon=2$	$\epsilon=4$	$\epsilon=8$	$\epsilon=16$	$k$	$\epsilon=.5$	$\epsilon=1$	$\epsilon=2$	$\epsilon=4$	$\epsilon=8$	$\epsilon=16$
1	78.46	72.07	66.02	59.72	48.61	23.71	1	98.26	97.36	96.03	92.97	86.89	77.14
2	<b>79.48</b>	<b>74.22</b>	<b>70.18</b>	<b>66.58</b>	<b>57.25</b>	26.23	2	98.32	97.45	<b>96.15</b>	<b>93.16</b>	<b>87.34</b>	<b>78.24</b>
4	78.82	72.71	67.82	63.60	54.80	<b>27.32</b>	4	98.30	97.30	95.81	92.34	84.89	72.48
8	78.00	70.45	64.24	59.01	50.32	26.24	8	<b>98.36</b>	<b>97.46</b>	95.96	92.33	83.70	69.33

(a) CIFAR-10 ( $\pm 0.6$  confidence)(b) MNIST ( $\pm 0.1$  confidence)

Figure 10: Adversarial data.

Results for CIFAR-10 with a Resnet18 architecture are in Figure 9. Numbers in this experiment are averaged over 20 Monte Carlo trials ( $\pm 0.03$  confidence on test performance). While manifold 1-mixup outperforms the standard 1-mixup from Figure 6, it is matched by manifold  $k$ -mixups with  $k = 4$  and outperformed by standard  $k$ -mixup (Figure 6,  $k = 8$ ). We also tried randomizing over (a) the outputs of all residual blocks and (b) the outputs of (lower-dimensional) deep residual blocks only, but found that performance of both 1-mixup and  $k$ -mixup degrades in these cases; this underscores that mixup in hidden layer manifolds is not guaranteed to be effective and can require tuning.

**Adversarial robustness.** Figure 10 shows performance results on white-box adversarial attacks generated by the FGSM method (implementation of [25]<sup>2</sup>) for various values of maximum adversarial perturbation. As in [9], we used FGSM over PGD, since the iterative PGD attacks are significantly more effective, making performance improvements seem less relevant in practice. We show CIFAR-10 % correct classification on white-box FGSM adversarial data (10000 points), where the maximum adversarial perturbation is set to  $\epsilon/255$ ; performance is averaged over 30 Monte Carlo trials ( $\pm 0.6$  confidence). All performances are without adversarial training. Note that  $k = 2$  outperforms  $k = 1$  uniformly by as much as 8.64%, and the  $k > 1$  mixups all outperform  $k = 1$  mixup on larger attacks.

Similar results for MNIST are in Figure 10(b), with the FGSM attacks being somewhat less effective. Here  $k = 8$  is best for smaller attacks, and  $k = 2$  is best for larger attacks.

The improved robustness shown by  $k$ -mixup speaks to one of the key goals of mixup, that of gently smoothing the predictions in the parts of the data space where no/few labels are available. This smoothness should, in theory, make adversarial attacks require greater magnitude to successfully “break” the model.

## 6 Conclusions and Future Work

The experiments above demonstrate that  $k$ -mixup often improves the generalization and robustness gains achieved by (1-)mixup, and does no harm in the worst case. It is simple to implement, adds little computational overhead to conventional (1-)mixup training, and may also be easily combined with related mixup variants. As  $k$  increases, the regularization induced more accurately reflects the local structure of the training data, especially in the manifold support and clustered settings, as argued in Sections 3 and 4.

Our experiments show the greatest improvement from using  $k$ -mixup on low-dimensional datasets, while the improvement on high-dimensional datasets remains positive but is smaller (recall that classic mixup also has somewhat small gains over no mixup in these settings). This difference could be due to the diminishing value of Euclidean distance for characterizing dataset geometry in high dimensions [26], but intriguingly this effect was not remedied by doing OT in the possibly lower-dimensional manifolds created by the higher layers in our manifold mixup experiments. To remedy this issue, in future work we will consider alternative metric learning strategies, with the goal of identifying effective high-dimensional metrics for displacement interpolation of data points.

Mixup has been incorporated into a broad range of learning applications, many of which we have not empirically investigated here. The original work demonstrated robustness to label corruption and improved GAN training stability, which could easily benefit from  $k$ -mixup as well. Additionally, mixup has been used for augmentation in semi-supervised learning [14, 13]. Given its simplicity, a  $k$ -mixup augmentation may be able to generate more informed shifts of labelled and unlabelled training points. This same philosophy applies to a recent method for generalizing fair classifiers [15], which already leverages manifold mixup.

<sup>2</sup>Software has MIT License

## References

- [1] Alex Krizhevsky, Ilya Sutskever, and Geoffrey E. Hinton. ImageNet classification with deep convolutional neural networks. In *Proceedings of the 25th International Conference on Neural Information Processing Systems - Volume 1*, NIPS, pages 1097–1105, Red Hook, NY, USA, December 2012.
- [2] Geoffrey Hinton, Li Deng, Dong Yu, George E. Dahl, Abdel-rahman Mohamed, Navdeep Jaitly, Andrew Senior, Vincent Vanhoucke, Patrick Nguyen, Tara N. Sainath, and Brian Kingsbury. Deep Neural Networks for Acoustic Modeling in Speech Recognition: The Shared Views of Four Research Groups. *IEEE Signal Processing Magazine*, 29(6):82–97, November 2012. Conference Name: IEEE Signal Processing Magazine.
- [3] David Silver, Aja Huang, Chris J. Maddison, Arthur Guez, Laurent Sifre, George van den Driessche, Julian Schrittwieser, Ioannis Antonoglou, Veda Panneershelvam, Marc Lanctot, Sander Dieleman, Dominik Grewe, John Nham, Nal Kalchbrenner, Ilya Sutskever, Timothy Lillicrap, Madeleine Leach, Koray Kavukcuoglu, Thore Graepel, and Demis Hassabis. Mastering the game of Go with deep neural networks and tree search. *Nature*, 529(7587):484–489, January 2016. Number: 7587 Publisher: Nature Publishing Group.
- [4] Yann LeCun, Yoshua Bengio, and Geoffrey Hinton. Deep learning. *Nature*, 521(7553):436–444, May 2015. Number: 7553 Publisher: Nature Publishing Group.
- [5] Dzmitry Bahdanau, Kyunghyun Cho, and Yoshua Bengio. Neural machine translation by jointly learning to align and translate. In *International Conference on Learning Representations*, 2015.
- [6] Chiyuan Zhang, Samy Bengio, Moritz Hardt, Benjamin Recht, and Oriol Vinyals. Understanding deep learning requires rethinking generalization. In *International Conference on Learning Representations*, 2017.
- [7] Christian Szegedy, Wojciech Zaremba, Ilya Sutskever, Joan Bruna, Dumitru Erhan, Ian Goodfellow, and Rob Fergus. Intriguing properties of neural networks. In *International Conference on Learning Representations*, 2014.
- [8] Hongyi Zhang, Moustapha Cisse, Yann N. Dauphin, and David Lopez-Paz. mixup: Beyond Empirical Risk Minimization. February 2018.
- [9] Vikas Verma, Alex Lamb, Christopher Beckham, Amir Najafi, Aaron Courville, Ioannis Mitliagkas, and Yoshua Bengio. Manifold Mixup: Learning Better Representations by Interpolating Hidden States. September 2018.
- [10] Hongyu Guo, Yongyi Mao, and Richong Zhang. MixUp as Locally Linear Out-of-Manifold Regularization. *Proceedings of the AAAI Conference on Artificial Intelligence*, 33(01):3714–3722, July 2019. Number: 01.
- [11] Sangdoon Yun, Dongyoon Han, Seong Joon Oh, Sanghyuk Chun, Junsuk Choe, and Youngjoon Yoo. CutMix: Regularization Strategy to Train Strong Classifiers With Localizable Features. pages 6023–6032, 2019.
- [12] Jang-Hyun Kim, Wonho Choo, and Hyun Oh Song. Puzzle Mix: Exploiting Saliency and Local Statistics for Optimal Mixup. In *International Conference on Machine Learning*, pages 5275–5285. PMLR, November 2020. ISSN: 2640-3498.
- [13] Kihyuk Sohn, David Berthelot, Nicholas Carlini, Zizhao Zhang, Han Zhang, Colin A. Raffel, Ekin Dogus Cubuk, Alexey Kurakin, and Chun-Liang Li. FixMatch: Simplifying Semi-Supervised Learning with Consistency and Confidence. *Advances in Neural Information Processing Systems*, 33:596–608, 2020.
- [14] David Berthelot, Nicholas Carlini, Ian Goodfellow, Nicolas Papernot, Avital Oliver, and Colin A Raffel. MixMatch: A Holistic Approach to Semi-Supervised Learning. In H. Wallach, H. Larochelle, A. Beygelzimer, F. d’Alché-Buc, E. Fox, and R. Garnett, editors, *Advances in Neural Information Processing Systems*, volume 32. Curran Associates, Inc., 2019.
- [15] Ching-Yao Chuang and Youssef Mroueh. Fair mixup: Fairness via interpolation. In *International Conference on Learning Representations*, 2021.
- [16] Linjun Zhang, Zhun Deng, Kenji Kawaguchi, Amirata Ghorbani, and James Zou. How Does Mixup Help With Robustness and Generalization? September 2020.

- [17] Luigi Carratino, Moustapha Cissé, Rodolphe Jenatton, and Jean-Philippe Vert. On Mixup Regularization. *arXiv:2006.06049 [cs, stat]*, June 2020. arXiv: 2006.06049.
- [18] JangHyun Kim, Wonho Choo, Hosan Jeong, and Hyun Oh Song. Co-mixup: Saliency guided joint mixup with supermodular diversity. In *International Conference on Learning Representations*, 2021.
- [19] Filippo Santambrogio. *Optimal Transport for Applied Mathematicians: Calculus of Variations, PDEs, and Modeling*. Progress in Nonlinear Differential Equations and Their Applications. Birkhäuser Basel, 2015.
- [20] Gabriel Peyré and Marco Cuturi. Computational Optimal Transport: With Applications to Data Science. *Foundations and Trends® in Machine Learning*, 11(5-6):355–607, February 2019. Publisher: Now Publishers, Inc.
- [21] Dimitris Bertsimas and John Tsitsiklis. *Introduction to Linear Optimization*. Athena Scientific, 1st edition, 1997.
- [22] Justin Solomon, Kristjan Greenewald, and Haikady N Nagaraja.  $k$ -variance: A clustered notion of variance. *arXiv preprint arXiv:2012.06958*, 2020.
- [23] Jonathan Weed and Francis Bach. Sharp asymptotic and finite-sample rates of convergence of empirical measures in wasserstein distance. *Bernoulli*, 25(4A):2620–2648, 2019.
- [24] Yann LeCun and Corinna Cortes. MNIST handwritten digit database. 2010.
- [25] Hoki Kim. Torchattacks: A pytorch repository for adversarial attacks. *arXiv preprint arXiv:2010.01950*, 2020.
- [26] Charu C Aggarwal, Alexander Hinneburg, and Daniel A Keim. On the surprising behavior of distance metrics in high dimensional space. In *International conference on database theory*, pages 420–434. Springer, 2001.
- [27] S. K. Katti. Moments of the Absolute Difference and Absolute Deviation of Discrete Distributions. *The Annals of Mathematical Statistics*, 31(1):78–85, 1960. Publisher: Institute of Mathematical Statistics.

## A Proof of Lemma 1

We argue by contradiction and prove the result for  $m = 2$  first. Suppose that the number of cross-cluster matchings exceeds  $|r_1 - s_1|$ . Then by the pigeonhole principle, there must be at least two such matchings, which we'll say are between  $p_i$  and  $q_i$ , and  $p_{i+1}$  and  $q_{i+1}$ , WLOG. As the cost of the cross-cluster matchings is  $\geq (2\Delta)^2$ , and the cost of intra-cluster matchings is  $\leq (2\Delta)^2$ , a more optimal matching would pair  $p_i$  and  $q_{i+1}$ , and  $p_{i+1}$  and  $q_i$ . This contradicts optimality of the initial pairing.

In the scenario with  $m$  clusters, an analogous argument works. As above,  $|r_i - s_i|$  is the number of cluster  $i$  elements that must be matched in a cross-cluster fashion, and half the sum of these quantities is the minimum number of cross-cluster matchings overall. If this number is exceeded, by the pigeonhole principle, there must be additional cross-cluster matches that form a cycle in the graph over clusters. As above, the cost would be reduced by matching points within the same clusters, so this contradicts optimality.

## B Proof of Theorem 1

We first prove the result for two clusters of weight  $p$  and  $1 - p$ . With our clustered assumption, we may assume that all identifications that can be intracluster will be intracluster. Thus, if  $s_1$  and  $s_2$  denote the number of points in cluster 1 from batch 1 and 2, then the resulting number of cross-cluster matches is  $|s_1 - s_2|$ . As the samples for our batches are i.i.d., these random variables follow a simple binomial distribution  $B(k, p)$ . We can bound the expectation of this quantity with Jensen's inequality:

$$(\mathbb{E}[|s_1 - s_2|])^2 \leq \mathbb{E}[|s_1 - s_2|^2] = 2 \text{Var}(s_1) = 2kp(1 - p)$$

With some algebraic manipulation, our desired rate bound results. It is also possible to get an exact rate with some hypergeometric identities [27], but these simply differ by a constant factor, so we leave omit the exact expressions here.

For the general case, our clustered assumption again allows us to assume that OT will prioritize intracluster identifications. Thus, if we let  $r_i$  and  $s_i$  denote the number of samples in cluster  $i$  in batch 1 and 2, respectively, then the number of cross-cluster matchings will be  $\frac{1}{2} \sum_i |r_i - s_i|$ . Ultimately,  $r_i$  and  $s_i$  are sampled from a binomial distribution  $B(k, p_i)$ , so we may repeat the argument above and note that  $\mathbb{E}[r_i = s_i] \leq \sqrt{2kp_i(1 - p_i)}$ . Simple algebraic manipulations lead to the desired result.

## C Proof of Theorem 2

By the smooth boundary and positive density assumptions, we know that  $P(A_\delta) > 0$  and  $P(B_\delta) > 0$  for any  $\delta > 0$ . Hence, for fixed  $\delta$  and  $k$  large enough (by Theorem 6), we know that with high probability the sets  $A_\delta$  and  $B_\delta$  each contain more points than the number of cross-cluster identifications.

Now consider  $A_\epsilon$  and  $B_\epsilon$  for  $\epsilon = 2\delta + (\max(R_A, R_B)^2)/(2D^2)$ . All cross-cluster matches need to be assigned. The cost of assigning a cross-cluster match to a point in  $A_\delta$  and a point in  $B_\delta$  is at most  $D^2(1 + 2\delta)^2$  (since we are using  $W_2$ ). Furthermore, the cost of assigning a cross-cluster match that contains a point in  $A$  outside  $A_\epsilon$  and an arbitrary point in  $B$  is at least  $D^2(1 + \epsilon)^2$ . Consider the difference between these two costs:

$$D^2(1 + \epsilon)^2 - D^2(1 + 2\delta)^2 = D^2(2(\epsilon - 2\delta) + \epsilon^2 - 4\delta^2) > 2D^2 \frac{\max(R_A, R_B)^2}{2D^2} \geq R_A^2.$$

Since this difference  $> 0$  and we have shown  $A_\delta$  contains sufficient points for handling all assignments, this assignment outside of  $A_\epsilon$  will only occur if there is a within-cluster pair which benefits from using the available point in  $A_\epsilon$  more than is lost by not giving it to the cross-cluster pair ( $> R_A^2$ ). The maximum possible benefit gained by the within-cluster pair is the squared radius of  $A$ , i.e.  $R_A^2$ . Since we have shown that the lost cost for the cross-cluster pair is bigger than  $R_A^2$ , we have arrived at a contradiction. The proof is similar for the  $B$  side.

We have thus shown that for  $k$  large enough (depending on  $\delta$ ), with high probability all cross-cluster matches have an endpoint each in  $A_\epsilon$  and  $B_\epsilon$  where  $\epsilon = 2\delta + (\max(R_A, R_B)^2)/(2D^2)$ . Setting  $\delta = (\max(R_A, R_B)^2)/(4D^2)$  completes the proof.

## D Proof of Theorem 3

We mostly follow the notation and argument of [16] (c.f. Lemma 3.1), modifying it for our setting. There they consider sampling  $\lambda \sim \text{Beta}(\alpha, \beta)$  from an asymmetric Dirichlet distribution. Here, we assume a symmetric Dirichlet distribution, such that  $\alpha = \beta$ , simplifying most of the expressions. The analogous results hold in the asymmetric case with simple modifications.

Consider the probability distribution  $\tilde{D}_\lambda$  with probability distribution:  $\beta(\alpha + 1, \alpha)$ . Note that this distribution is more heavily weighted towards 1 across all  $\alpha$ , and for  $\alpha < 1$ , there is an asymptote as you approach 1.

Let us adopt the shorthand notation  $\tilde{x}_{i, \sigma_{\gamma\xi}(i)}(\lambda) := \lambda x_i^\gamma + (1 - \lambda)x_{\sigma_{\gamma\xi}}^\xi$  for an interpolated feature point. The manipulations below are abbreviated, as they do not differ much for our generalization.

$$\begin{aligned} \mathcal{E}_k^{mix}(f) &= \frac{1}{k \binom{N}{k}^2} \mathbb{E}_{\lambda \sim \beta(\alpha, \alpha)} \sum_{\gamma, \xi=1}^k \sum_{i=1}^k h(f(\tilde{x}_{i, \sigma_{\gamma\xi}(i)}(\lambda))) - (\lambda y_i^\gamma + (1 - \lambda)y_{\sigma_{\gamma\xi}}^\xi) f(\tilde{x}_{i, \sigma_{\gamma\xi}(i)}(\lambda)) \\ &= \frac{1}{k \binom{N}{k}^2} \mathbb{E}_{\lambda \sim \beta(\alpha, \alpha)} \mathbb{E}_{B \sim \text{Bern}(\lambda)} \sum_{\gamma, \xi=1}^k \sum_{i=1}^k B[h(f(\tilde{x}_{i, \sigma_{\gamma\xi}(i)}(\lambda))) - y_i^\gamma f(\tilde{x}_{i, \sigma_{\gamma\xi}(i)}(\lambda))] \\ &\quad + (1 - B)[h(f(\tilde{x}_{i, \sigma_{\gamma\xi}(i)}(\lambda))) - y_{\sigma_{\gamma\xi}}^\xi f(\tilde{x}_{i, \sigma_{\gamma\xi}(i)}(\lambda))] \\ &= \frac{1}{k \binom{N}{k}^2} \sum_{\gamma, \xi=1}^k \sum_{i=1}^k \mathbb{E}_{\lambda \sim \beta(\alpha+1, \alpha)} h(f(\tilde{x}_{i, \sigma_{\gamma\xi}(i)}(\lambda))) - y_i^\gamma f(\tilde{x}_{i, \sigma_{\gamma\xi}(i)}(\lambda)) \end{aligned}$$

For the third equality above, the ordering of sampling for  $\lambda$  and  $B$  has been swapped via conjugacy:  $\lambda \sim \beta(\alpha, \alpha)$ ,  $B|\lambda \sim \text{Bern}(\lambda)$  is equivalent to  $B \sim \mathcal{U}\{0, 1\}$ ,  $\lambda|B \sim \beta(\alpha + B, \alpha + 1 - B)$ . This is combined with the fact that  $\tilde{x}_{i, \sigma_{\gamma\xi}(i)}(1 - \lambda) = \tilde{x}_{\sigma_{\gamma\xi}(i), i}(\lambda)$  to get the last line above.

Now we can swap the sums, grouping over the initial point to express this as the following:

$$\mathcal{E}_k^{mix}(f) = \frac{1}{N} \sum_{i=1}^N \mathbb{E}_{\lambda \sim \beta(\alpha+1, \alpha)} \mathbb{E}_{r \sim \mathcal{D}_i} h(f(\lambda x_i + (1 - \lambda)r)) - y_i^\gamma f(\lambda x_i + (1 - \lambda)r),$$

where the probability distribution  $\mathcal{D}_i$  is as described in the text.

The remainder of the argument performs a Taylor expansion of the loss term  $h(f(\lambda x_i + (1 - \lambda)r)) - y_i^\gamma f(\lambda x_i + (1 - \lambda)r)$  in terms of  $1 - \lambda$ , and is not specific to our setting, so we refer the reader to Appendix A.1 of [16]. for the argument.

## E Proof of Theorem 4

This argument is modelled on a proof in [17], so we adopt analogous notation and highlight the differences in our setting and refer the reader to Appendix B.1 of that paper for any omitted details. First, let us use shorthand notation for the interpolated loss function:

$$m_i^{\gamma\xi}(\lambda) = \ell(f(\lambda x_i^\gamma + (1 - \lambda)x_{\sigma_{\gamma\xi}(i)}^\xi), \lambda y_i^\gamma + (1 - \lambda)y_{\sigma_{\gamma\xi}(i)}^\xi).$$

Then the mixup objective may be written as:

$$\mathcal{E}_k^{mix}(f) = \frac{1}{k \binom{N}{k}^2} \sum_{\gamma, \xi=1}^k \sum_{i=1}^k \mathbb{E}_\lambda m_i^{\gamma\xi}(\lambda).$$

As  $\lambda \sim \beta(\alpha, \alpha)$ , we may leverage the symmetry of the sampling function and use a parameter  $\theta \sim \beta_{[1/2, 1]}(\alpha, \alpha)$  to write the objective as:

$$\mathcal{E}_k^{mix}(f) = \frac{1}{\binom{N}{k}} \sum_{\gamma=1}^k \ell_i, \quad \text{where } \ell_i = \frac{1}{k \binom{N}{k}} \sum_{\xi=1}^k \sum_{i=1}^k \mathbb{E}_\theta m_i^{\gamma\xi}(\theta)$$

To obtain the form of the theorem in the text, we introduce auxiliary variables  $\tilde{x}_i^\gamma, \tilde{y}_i^\gamma$  to represent the mean-reverted training points:

$$\begin{aligned} \tilde{x}_i^\gamma &= \mathbb{E}_{\theta, \xi} \left[ \theta x_i^\gamma + (1 - \theta) x_{\sigma_{\gamma\xi}(i)}^\xi \right] \\ \tilde{y}_i^\gamma &= \mathbb{E}_{\theta, \xi} \left[ \theta y_i^\gamma + (1 - \theta) y_{\sigma_{\gamma\xi}(i)}^\xi \right], \end{aligned}$$

and  $\tilde{\delta}_i^\gamma, \tilde{\epsilon}_i^\gamma$  to denote the zero mean perturbations about these points:

$$\begin{aligned} \tilde{\delta}_i^\gamma &= \theta x_i^\gamma + (1 - \theta) x_{\sigma_{\gamma\xi}(i)}^\xi - \mathbb{E}_{\theta, \xi} \left[ \theta x_i^\gamma + (1 - \theta) x_{\sigma_{\gamma\xi}(i)}^\xi \right] \\ \tilde{\epsilon}_i^\gamma &= \theta y_i^\gamma + (1 - \theta) y_{\sigma_{\gamma\xi}(i)}^\xi - \mathbb{E}_{\theta, \xi} \left[ \theta y_i^\gamma + (1 - \theta) y_{\sigma_{\gamma\xi}(i)}^\xi \right]. \end{aligned}$$

These reduce to the simplified expressions given in the theorem if we recall that  $\theta$  and  $\xi$  are independent random variables. Note that both the mean-reverted points and the perturbations are informed by the local distribution  $\mathcal{D}_i$ .

### E.1 Covariance structure

As in [17], it's possible to come up with some simple expressions for the covariance structure of the local perturbations, so we write out the analogous result below. As the argument is very similar, we omit it.

**Lemma 2.** Let  $\sigma^2$  denote the variance of  $\beta_{[1/2,1]}(\alpha, \alpha)$ , and  $\nu^2 := \sigma^2 + (1 - \bar{\theta})^2$ . Then the following expressions hold for the covariance of the zero mean perturbations:

$$\begin{aligned}\mathbb{E}_{\theta, \xi} \tilde{\delta}_i^\gamma (\tilde{\delta}_i^\gamma)^\top &= \frac{\sigma^2 (\tilde{x}_i^\gamma - \bar{x}_i^\gamma) (\tilde{x}_i^\gamma - \bar{x}_i^\gamma)^\top + \nu^2 \Sigma_{\tilde{x}_i^\gamma \tilde{x}_i^\gamma}}{\bar{\theta}^2} \\ \mathbb{E}_{\theta, \xi} \tilde{\epsilon}_i^\gamma (\tilde{\epsilon}_i^\gamma)^\top &= \frac{\sigma^2 (\tilde{y}_i^\gamma - \bar{y}_i^\gamma) (\tilde{y}_i^\gamma - \bar{y}_i^\gamma)^\top + \nu^2 \Sigma_{\tilde{y}_i^\gamma \tilde{y}_i^\gamma}}{\bar{\theta}^2} \\ \mathbb{E}_{\theta, \xi} \tilde{\delta}_i^\gamma (\tilde{\epsilon}_i^\gamma)^\top &= \frac{\sigma^2 (\tilde{x}_i^\gamma - \bar{x}_i^\gamma) (\tilde{y}_i^\gamma - \bar{y}_i^\gamma)^\top + \nu^2 \Sigma_{\tilde{x}_i^\gamma \tilde{y}_i^\gamma}}{\bar{\theta}^2},\end{aligned}$$

where  $\Sigma_{\tilde{x}_i^\gamma \tilde{x}_i^\gamma}, \Sigma_{\tilde{y}_i^\gamma \tilde{y}_i^\gamma}, \Sigma_{\tilde{x}_i^\gamma \tilde{y}_i^\gamma}$  denote empirical covariance matrices.

Note again, that the covariances above are locally-informed, rather than globally determined. Lastly, there is also a quadratic expansion performed about the mean-reverted points  $\tilde{x}_i^\gamma, \tilde{y}_i^\gamma$  with terms that regularize  $f$ , but we omit this result as the regularization of Theorem 3 is more intuitive (c.f. Theorem 2 of [17]).